BiSpectral Contactless hand based biometric identification device

Chapter · July 2011

DOI: 10.5772/18096 · Source: InTech

2 authors:

Aythami Morales
Universidad Autónoma de Madrid
173 PUBLICATIONS **2,021** CITATIONS

SEE PROFILE

Miguel A. Ferrer
Universidad de Las Palmas de Gran Canaria
296 PUBLICATIONS **3,633** CITATIONS

SEE PROFILE

14

BiSpectral Contactless Hand Based Biometric Identification Device

Aythami Morales and Miguel A. Ferrer
Instituto para el Desarrollo Tecnológico y la Innovación en Comunicaciones (IDeTIC), Universidad de Las Palmas de Gran Canaria, Spain

1. Introduction

Biometrics plays an increasingly important role in authentication and identification systems. The process of biometric recognition allows the identification of individuals based on the physical or behavioral characteristics. Among the most common biometric features used are fingerprint, iris, face, voice, signature and hand. Hand based biometric systems exhibit many desirable characteristics when working with low resolution sensors (which are most appropriate for civil and commercial applications), including low cost sensors, acceptable indentification performance, robustness to environmental conditions and individual anomalies, and high speed identification algorithms. For higher security applications such as forensics, high resolution images are more suitable (Jain et al, 2001) (Konga et al, 2009).

Most hand-based biometric schemes in the literature are based on measuring the hand silhoutte as a distinctive personal attribute for an authentication task. First it was accomplished using guiding pegs mounted on a flat surface of the imaging device (Sanchez-Reillo et al, 2000) (Jain et al, 1999). Although the guiding pegs provide consistent measuring positions, they cause some problems as well: 1) The pegs can deform the shape of a hand (Wong & Shi, 2002) and 2) The users must be well trained to cooperate with the system. Thus, peg-free hand geometry techniques were considered giving the hand some motion freedom (Bulatov et al, 2004).

There are two main approaches for geometrical features extraction; those based on measure the finger lengths and widths at various positions, palm size, etc. and another based on represent the global hand shape (Öden et al, 2003) (Yörük et al, 2006). Both approaches use the finger tip points and the finger valley points as the landmarksfor image alignment.

The palm texture can be also used as biometric trait for personal identification. It can be used both by itself (Han et al, 2003) (Ribarić & Fratric, 2005) (Sun et al 2005) (Kong & Zhang, 2004) (Badrinath & Gupta, 2009) or combined with hand shape (Ribaric et al, 2003) (Li et al, 2006) (Kumar et al, 2006) (Kumar & Zhang, 2004) at score level or at representation level. Although fusion increases accuracy, it generally increases computation costs and template sizes and reduces user acceptance.

Recently, perhaps due to hygiene consideration, contact-free hand biometric systems have been proposed. The two main issues to be dealt with in a contact-free system are hand segmentation and the projective distortions associated with the absence of the contact plane.

Previous research on contactless systems includes (Haeger, 2003), where once the centroid of a segmented hand was detected a number of concentric circles were drawn around the centroid passing through the fingers. Using these circles 124 different finger sizes were measured and used for biometric identification with limited results. (Hao et al, 2008) proposes a contactless biometric system based on a fusion of palm texture and palm vein pattern based on feature level and image level fusion. To realize the acquisition the user introduces the hand in a black box. Therefore illumination and background were controlled. The use of such black box can raise concerns or unwillingly scare the users and lower the user acceptance. Doi and Yamanaka (Doi et al, 2003) created a mesh of a hand image captured by an infrared CCD camera. The mesh was created using 20 to 30 feature points extracted from the principal creases of the fingers and palm. Root-mean-square (rms) deviation was used to measure the alignment distance between the meshes, which was was also sensitive to perspective distortion. In reference (Morales et al, 2008), the contactless hand geometry system able to obtain images in non controlled environments is investigated. The hand geometry based feature extraction methods show poor results due to projective distortion problems. Palmprint authentication based on contactless imaging was proposed in (Morales et al 2010). In this chapter was proposed a combined method based on two palm features approaches. The combination with an uncorrelated biometric as hand geometry was mentioned as future work.
As result of the above experience, the aim of this chaper is get together all the previous experience and propose a contact-free biometric system based on the combination of hand geometry and palmprint using only low cost devices for medium security environments. The device uses infrared illumination and infrared camera to reduce some problems as changing lighting conditions or complex background containing surfaces and objects with skin-like colors. To acquire the the palm texture information a second camera in the visible band is added. The visible image can then be segmented using the information from the infrared camera. We propose the use of Active Shape Models to correlate the hand contourns from the infrared and visible images. The projective distortion problem is alleviated using a template guide on the video screen. The verification methodology includes 1000 hand images from a database acquired with the proposed device.
The outline of the chapter is as follows. In the next section we will introduce the proposed bispectral contactless hand-based biometric device. Section III describes the geometry parameters and Section IV presents the palmprint approaches based on OLOF and MSIFT. Section V presents our experimental results we assess the proposed device. The chapter is closed with conclusions, acknowledgements and references.

2. Acquisition device

The acquisition device used consists of two inexpensive, standard web cams that obtain images of the hand at the same time. The so called infrared (IR) webcam acquires images in the infrared band (750 to 1000nm) and the so called visible (V) camera acquires images in the visible range (400 to 700nm).
The IR webcam was created by simply taking out the webcam lens that eliminates the infrared radiation and adding a filter that eliminates the visible band. We used Kodak filter No 87 FS4-518 and No 87c FS4-519 with no transmittance below 750 nm.
The images of the IR webcam were used for hand geometry. So, we increase the image contrat by setting the IR webcam specification as follows: maximum value of contrast and low values of brightness, gain and exposure time. An example of the image acquired can be seen in Figure 1.

Fig. 1. Left, hand acquired with a standard webcam; right, hand acquired with the IR webcam.

The infrared illumination is composed of a set of 24 GaAs infrared emitting diode (CQY 99) with a peak wavelength emission of 925 nm and a spectral bandwidth of 40 nm. The diodes were placed in an inverted U shape with the IR and V webcams in the middle (see Figure 2). The open part of the U shape will coincide with the wrists of the hand image. The focus of the IR webcam lens is adjusted manually the first time the webcam is used.

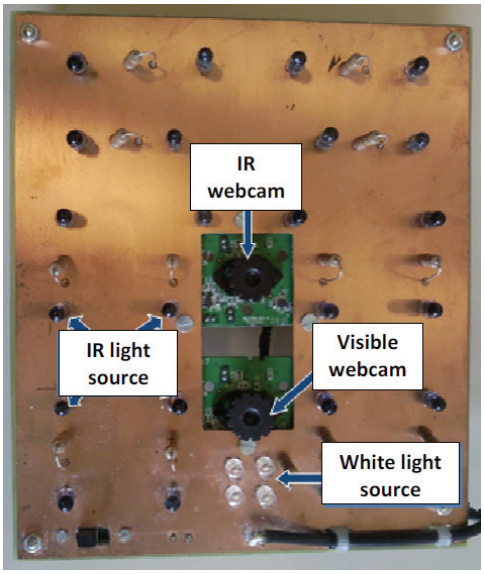

Fig. 2. Bispectral hand based biometric system

To alleviate the projective distortion of the hand image acquired we used a hand mask in the video screen of the computer: the user places his or her hand over the camera and adjusts the position and pose of the hand in order to overlap with the hand mask drawn on the device screen. When the hand and mask overlap more than 70%, the device automatically acquires both the IR and visible image. An example of this process can be seen in Figure 3. The mask used was the averaged hand silhouette from the GPDS hand database scaled to the webcam resolution and dilated with a 30 by 30 structuring element.

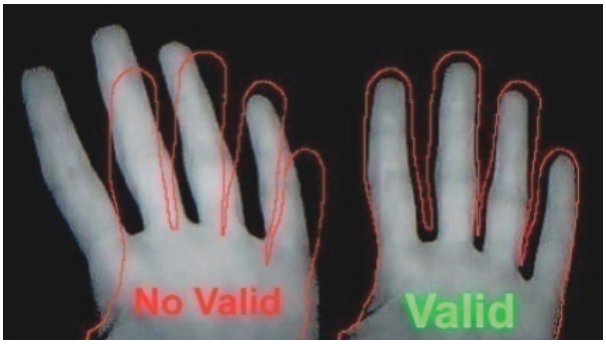

Fig. 3. Hand mask and hand overlapping. Valid stands for overlapping greater than 70%.

The V webcam used for palm print biometries is located just 2 centimeters below the IR webcam. The settings of the V webcam are configurated by default. The lens focus is adjusted manually the first time it is used. The illumination consists of a set of 4 white LEDs emitting in the 400nm to 700nm band. An example of images acquired can be seen in Figure 4.

Fig. 4. Left: image acquired by the IR webcam, right: visible image of the hand palm.

3. Geometrical hand biometries

Due to the webcam setup and IR illumination, a reliable hand contour can be obtained binarizing the IR image with its Otsu's threshold.

To work out the tips and valleys between the fingers we convert the Cartesian coordinates of the contour to polar coordinates (radius and angle) considering the center of the image base as the coordinates origin. The peaks in the radius coordinate locate the provisional position of the finger tips and the minima of the radius indicate the valleys between fingers. Let and $\varphi_c(i), 1 \le i \le L$ the radius and angle of the i^{th} hand contour pixel. The index i_p^j of the i^{th} radius peaks are obtained as:

$$i_p^j \in peak \quad if\ r_c\left(i_p^j\right) = \max\left\{r_c(i) \middle| i_p^j - 100 \le i \le i_p^j + 100\right\} \tag{1}$$

With $101 < i_p^1 < i_p^2 < \ldots < i_p^5 < L - 100$. If the number of radius peaks obtained is greater than 5, we suppose than the hand detector has been fault and go to hand detection module waiting for a hand. As the hand is expected, i_p^1 corresponds to the little finger tip.

The index i_v^j of the j^{th} valley is worked out as:

$$i_v^j \in valley \quad if\ r_c\left(i_v^j\right) = \min\left\{r_c(i)\middle| i_p^j \le i \le i_p^{j+1}\right\} \tag{2}$$

The exterior base of the index and little fingers are obtained as the nearest pixel of the exterior contour to the valley between the index and middle fingers and the valley between the index and little fingers, respectively, i.e.:

$$i_{index} \in valley \quad if\ i_{index} = \arg\min_i \left\{ d(\langle x_c(i), y_c(i)\rangle, \langle x_c(i_v^3), y_c(i_v^3)\rangle) \middle| i_p^5 \le i \le i_v^4 \right\} \tag{3}$$

$$i_{little} \in valley \quad if\ i_{little} = \arg\min_i \left\{ d(\langle x_c(i), y_c(i)\rangle, \langle x_c(i_v^1), y_c(i_v^1)\rangle) \middle| 1 \le i \le i_p^1 \right\} \tag{4}$$

Being $d(\cdot,\cdot)$ the Euclidean distance. We will call $i_v^1 = i_{little}$, and $i_v^5 = i_{index}$.

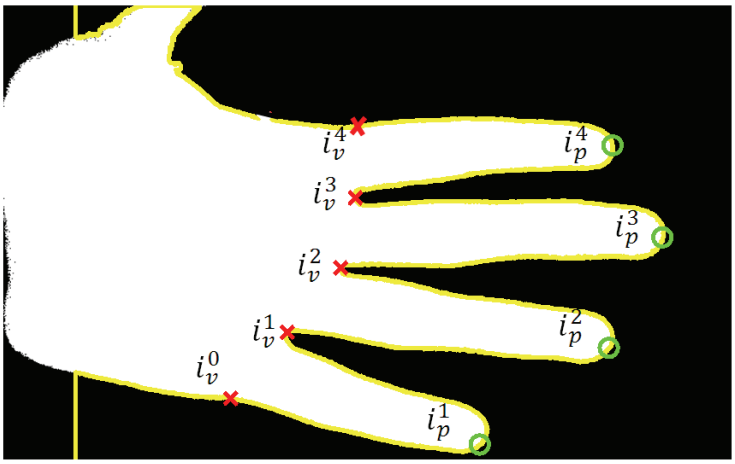

Fig. 5. Tips, valleys and exteriors of fingers localization

The position of the tip of the finger is finely adjusted as follow. The lines that minimize the square error with each side finger contour are obtained as follows:

1. Four equal spaced points are selected from the 35% to the 80% of each finger side. The 35% is selected to avoid the presence of rings, and the 80% is selected to avoid the tip curvature of the finger tip. For the right side of the finger, the four points are calculated as $i_{rfs}^j = (i_p^j - i_p^{j-1}) * C(k) + i_v^{j-1}$, being $C(k) = \{0.35, 0.50, 0.65, 0.80\}$, and for the left finger side are calculated as $i_{lfs}^j(k) = (i_v^{j+1} - i_p^j) * C(k) + i_p^j$.
2. The lines that minimize the square error with the selected point of each finger side are calculated. For the right side, the line is defined as $y = m_r^j \cdot x + b_r^j$, being b_r^j and m_r^j calculated as:

$$\begin{pmatrix} b_r^j \\ m_r^j \end{pmatrix} = pinv \begin{pmatrix} 1 & x(i_{rfs}^j(1)) \\ 1 & x(i_{rfs}^j(2)) \\ 1 & x(i_{rfs}^j(3)) \\ 1 & x(i_{rfs}^j(4)) \end{pmatrix} \cdot \begin{pmatrix} y(i_{rfs}^j(1)) \\ y(i_{rfs}^j(2)) \\ y(i_{rfs}^j(3)) \\ y(i_{rfs}^j(4)) \end{pmatrix} \tag{5}$$

being pinv the pseudoinverse. For the left side, the line $y = m_l^j \cdot x + b_l^j$ is obtained as above using $i_{rfs}^j(k)$, Fig 6.

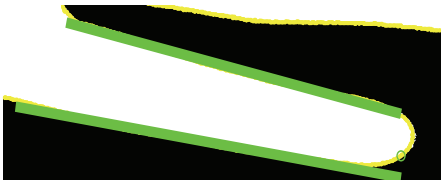

Fig. 6. Finger contour line approximation $y = m_r^j \cdot x + b_r^j$ and $y = m_l^j \cdot x + b_l^j$

3. The average of the two lines is considered the finger axis and calculated as $y = m_a^j \cdot x + b_a^j$ being $m_a^j = (m_r^j + m_l^j)/2$ and $b_a^j = (b_r^j + b_l^j)/2$, see Fig 7.

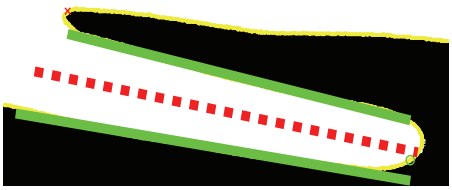

Fig. 7. Finger axis caluculation.

4. The tip of the finger is the point where the finger axis and the finger contour intersect, Fig 8.

$$i_p^j = \arg\min_i \left\{ d(\langle x_c(i), y_c(i) \rangle, y = m_a^j \cdot x + b_a^j) \middle| i_v^{j-1} \le i \le i_v^{j+1} \right\} \tag{6}$$

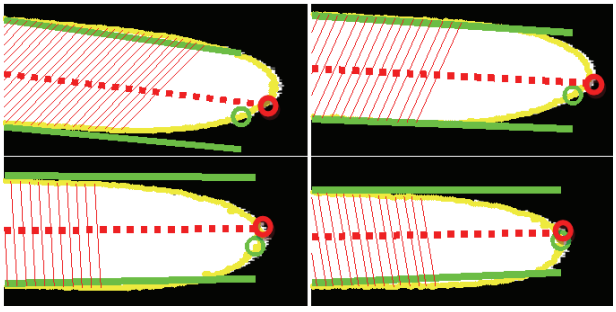

Fig. 8. In green initial tip localization; in red accurate tip localization.

The geometric features are obtained by measuring the widths of each finger. It is done as follows: The center base of each the finger $\left\langle x_{fb}^{j}, y_{fb}^{j} \right\rangle$ is defined as the point where the finger axis $y = m_a^j \cdot x + b_a^j$ intersects the finger base line

$$y = \frac{y(i_v^j) - y(i_v^{j-1})}{x(i_v^j) - x(i_v^{j-1})}(x - x(i_v^{j-1})) + y(i_v^{j-1}) \tag{7}$$

We select 12 equal space points between $\left\langle x_{fb}^{j}, y_{fb}^{j} \right\rangle$ and $\left\langle x_c(i_p^j), y_c(i_p^j) \right\rangle$ as follows:

$$x_s^j = (x_c(i_p^j) - x_{fb}^j) * C(k) + x_{fb}^j \tag{8}$$

$$y_s^j(k) = m_a^j \cdot x_s^j(k) + b_a^j \tag{9}$$

with $C(k) = \{0.20, 0.26, 0.32, \ldots, 0.80, 0.86\}$.

The perpendicular line to the finger axe is obtained in this point as

$$y = \frac{-1}{m_a^j}(x - x_s^j(k)) + y_s^j(k) = m_{pa}^j \cdot x + b_{pa}^j \tag{10}$$

The nearest contour points this line

$$i_{cr}^j(k) = \arg\min_i \left\{ d(\langle x_c(i), y_c(i) \rangle, y = m_{pa}^j \cdot x + b_{pa}^j) \middle| i_v^{j-1} \le i \le i_p^j \right\} \tag{11}$$

and

$$i_{cl}^j(k) = \arg\min_i \left\{ d(\langle x_c(i), y_c(i) \rangle, y = m_{pa}^j \cdot x + b_{pa}^j) \middle| i_v^j \le i \le i_v^j \right\} \tag{12}$$

Being the width at this point $d_w^j(k) = d(\langle x_c(i_{cr}), y_c(i_{cr}) \rangle, \langle x_c(i_{cl}), y_c(i_{cl}) \rangle)$. The geometric features are obtained by measuring 100 widths of each finger from the 15% to 85% of the finger length. An example can be seen in figure 9.

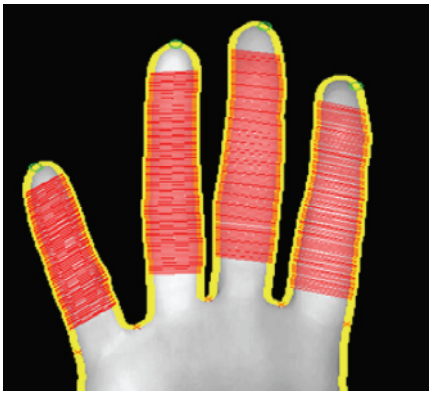

Fig. 9. Finger widths measured for the geometrical template

The width measures of the four fingers are concatenated resulting in a vector of 400 components $d_w^j(k), 1 \le j \le 4, 1 \le k \le 100$. The maximum of the vector is normalized to 1 to reduce the projection distortion and its average substracted. In order to reduce the dimensionality of the vector, the DCT transform is applied and the geometrical hand template is obtained by selecting from the 2nd to the 50th coefficients of the DCT transform.

As verifier we have used a Least Squares Support Vector Machine (LS-SVM). SVMs have been introduced within the context of statistical learning theory and structural risk minimization. Least Squares Support Vector Machines (LS-SVM) are reformulations to standard SVMs which lead to solving linear KKT systems. Robustness, sparseness, and weightings can be imposed to LS-SVMs where needed and a Bayesian framework with three levels of inference is then applied (Suykens et al, 2002).

The meta-parameters of the LS-SVM model are the width of the Gaussian kernels σ and the regularization factor γ. The regularization factor is taken as $\gamma = 20$ and is identical for all the LS-SVM models used here. The Gaussian width σ parameter is optimized as follows: the training sequence is randomly partitioned into two equal subsets $P_i, 1 \le i \le 2$. The LS-SVM is trained $L = 30$ times with the first subset P_1, $\gamma = 20$ and Gaussian width equal to L logarithmically equally spaced values between 10^1 and 10^4 $\sigma_l, 1 \le l \le L$. Each one of the L LS-SVM models is tested with the second subset P_2 obtaining L Equal Error Rate $EER_l, 1 \le l \le L$ measures and their associated thresholds $TEER_l, 1 \le l \le L$. As the positive samples are trained with target output +1 and the negative samples with target value -1, the threshold is limited to values between $-1 \le TEER_l \le 1$. The Gaussian width σ of the signature model and its decision threshold $TEER$ are obtained as $\sigma = \sigma_j$ and $TEER = (TEER_j + 1) \cdot 0.8 - 1$, where $j = \arg\min_{1 \le l \le L} \{EER_l\}$. Finally, the user hand model is obtained training the LS-SVM with all the training sequence.

To verify that an input image belongs to the claimed used, we calculated the score of the LS-SVM that models the claimed user. If the score is greater than the claimed user $TEER$, it is accepted as genuine.

4. Palm print subsystem

4.1 Hand segmentation

To extract the palm texture we use the visible image of the hand. The major problem in the visible image is the hand segmentation to obtain an invariable area of the hand palm. As the relation between the pixels of both images is variable depending of the distance from the camera to the hand, the contour obtained by the IR image is taken as initial guess of the hand contour in the visible image and the orientation, scale, position, and shape of the IR contour is adjusted to the visible image using an Active Shape Model (ASM) (Cootes et al, 1995).

ASMs are flexible models of image structures whose shape can vary. The models are able to capture the natural variability within a class of shapes, in this case hands, and can then be used for image segmentation (in addition to other applications). The ASM model was constructed from a dataset of 500 hand contours from the first 50 users of the GPDShand database (Ferrer et al, 2007).

For the point distribution models of the contours, we selected as landmark points the valley of the fingers. Between each pair of consecutive landmark points we selected 70 additional

points. In the trained model 96% of the variance could be explained by the first 9 eigenvectors or modes of variation.
Trained the ASM model, to segment the hand in the visible image, the landmarks and point between landmarks are obtained over the contour of the acquired hand in the IR image and they are displaced, rotated and distorted inside the ASM limits looking for edges in the visible image.The edges of the visible images were obtained summing the morphological gradient of the red, green and blue images. Figure 10 shows the results at the initial and final stages of the algorithm.

Fig. 10. Visible image, dotted line: initial contour, solid line: final contour..

4.2 Palmprint texture parameterization

The Orthogonal Line Ordinal Features (OLOF) method was originally introduced in (Sun et al, 2005) and was investigated for the palmprint feature extraction. The comparison of OLOF method with several other competing methods (Kong & Zhang, 2004) in this reference suggests the superiority of OLOF with such competitive feature extraction methods. The OLOF presented significantly improvement results but on conventional databases that are acquired from constrained imaging.
This method is based on 2D Gaussian filter to obtain the weighted average intensity of a line-like region. Its expression is as follows:

$$f(x,y,\theta)=\exp\left[-\left(\frac{x\cos\theta+y\sin\theta}{\delta_x}\right)^2-\left(\frac{-x\sin\theta+y\cos\theta}{\delta_y}\right)^2\right] \tag{13}$$

where θ denotes the orientation of 2D Gaussian filter, δ_x denotes the filter's horizontal scale and δy denotes the filter's vertical scale parameter. There no signicicant differences on results in the range $\delta_x, \delta_y \in [0.5-10]$. We empirically selected the parameters as δ_x = 5 and δ_y = 1.
To obtain the orthogonal filter, two Gaussian filters are used as follows:

$$OF(\theta)=f(x,y,\theta)-f(x,y,\theta+\frac{\pi}{2}) \tag{14}$$

Each palm image is filtered using three ordinal filters, $OF(\theta)$, $OF(\pi/6)$ and $OF(\pi/3)$ to obtain three binary masks based on a zero binarization threshold. In order to ensure the robustness against brightness, the discrete filters $OF(\theta)$, are turned to have zero average. Once filtered the central portion for images is cropped and binarized giving a value of 1 to 25% of the highest gray level pixels and the rest reset to 0 values. Finally, the three images are reduced to 50x50pixels. An example of this image can be seen in Figure 11.

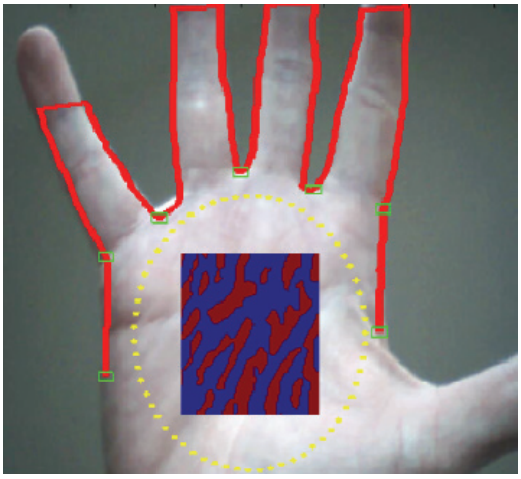

Fig. 11. Invariant area of the hand palm and the OLOF features overlapped to the palm

To verify that an input texture Q belongs to the identity with image texture (template) P we have used a normalized Hamming measure which can be described as:

$$D = 1 - \frac{\sum_{i=1}^{2n+1}\sum_{j=1}^{2n+1} P(i,j) \otimes Q(i,j)}{(2n+1)^2} \tag{15}$$

where the boolean operator $\otimes$ is equal to zero if and only if the two bits $P(i,j)$ and $Q(i,j)$ are equals. It is noted that D is between 0 and 1 (best matching). Because of the imperfect preprocessing, we need to vertically and horizontally translate one of the features a range of 4 to 4 and match again. The maximum D value obtained is considered to be the final matching score. If the matching score is greater than a threshold, the hand is accepted.

4.3 Palmprint MSIFT parameterization

The Scale Invariant Feature Transform was originally proposed in (Lowe, 2004). The features extracted are invariant to image scaling, rotation, and partially invariant to change in illumination and projective distortion. The SIFT is a feature extraction method based on the extraction of local information. The figure 12 resume the major stages to generate the set of features proposed by Lowe and our proposal to adapt it to palmprint contactless biometric systems called MSIFT.

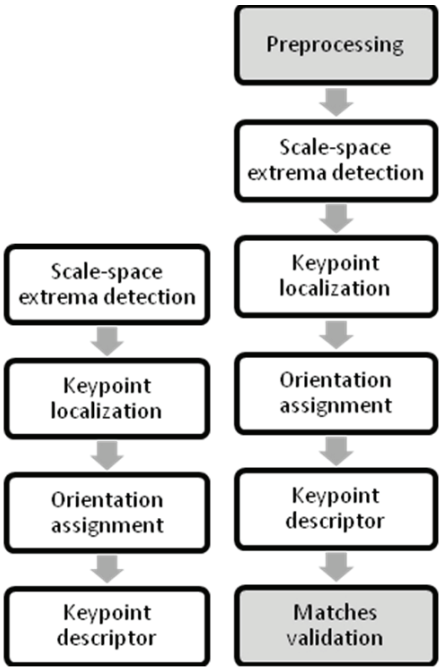

Fig. 12. On the Left the Lowe (Lowe, 2004) SIFT approach; on the right the contactless palmprint MSIFT approach proposed on this chapter.

The SIFT algorithm is based on detecting keypoints with similar propierties that are present in the reference and questioned image. In palmprint images acquired contactless from hand on movement with CMOS sensors of low quality, the images include blurring and several above mentioned distortion that reduce the ability of the SIFT algorithm to detect common keypoints. To alleviate such a problem we propose a preprocessing that highlight the interesting keypoints. The algorithm that preprocesses the image previous the application of the SIFT algorithm is called by us Modified SIFT (MSIFT) and consist of 6 steps:

Step 1. **Preprocessing:** In this chapter we propose a Gabor preprocessing to add robustness to SIFT approach. Assuming that the reference and questioned hand have similar orientation inside the image which is achieve during the segmentation stage. The real 2D Gabor filter used to process the palmprint image is defined by:

$$G(x,y,\theta,u,\varphi)=\frac{1}{2\pi\varphi^2}\exp\left\{-\frac{x^2+y^2}{2\varphi^2}\right\}\cos\{2\pi(ux\cos\theta+uy\sin\theta)\} \tag{16}$$

where u is the frequency of the sinusoidal wave, θ defines the orientation selectivity of the function, and φ is the standard deviation of the Gaussian envelope. In this chapter we used a Gabor filter setting with $\theta=0$, $\varphi=2.0$ and $u=0.1$. Greater robustness against brightness variation is assured by turning the discrete Gabor filter to average zero.

$$G^{'}(x,y,\theta,u,\varphi) = G(x,y,\theta,u,\varphi) - \frac{\sum_{i=1}^{2n+1}\sum_{j=1}^{2n+1} G(i,j,\theta,u,\varphi)}{(2n+1)^2} \tag{17}$$

Step 2. **Scale-space extrema detection:** It is applied over all scales and image locations. It is based on difference-of-Gaussian function to identify potential interest points that are invariant to scale and orientation. The input data is transformed to the space $L(x,y,\sigma)$ as follows:

$$L(x,y,\sigma) = g(x,y,\sigma) * I^{'}(x,y) \tag{18}$$

where $*$ corresponds to convolution operator, $I^{'}(x,y)$ is the preprocessed input image and $g(x,y,\sigma)$ is a Gaussian function with bandwidth σ. The difference-of-Gaussian function is defined as:

$$D(x,y,\sigma) = (g(x,y,k\sigma) - g(x,y,\sigma)) * I^{'}(x,y) = L(x,y,k\sigma) - L(x,y,\sigma) \tag{19}$$

Step 3. **Keypoint localization:** A detailed model is fit to determine location and scale of each candidate location. The interpolation is done using the quadratic Taylor expansion of the Difference-of-Gaussian scale-space function $D(x,y,\sigma)$ with the candidate keypoint as the origin. This Taylor expansion is given by:

$$D(x) = D + \frac{\partial D^T}{\partial x} + \frac{1}{2} x^T \frac{\partial^2 D^T}{\partial x^2} x \tag{20}$$

where the maxima and minima of D and its derivatives are evaluated at the candidate keypoint and $x = (x,y,\sigma)$ is the offset from this point, Fig 13.

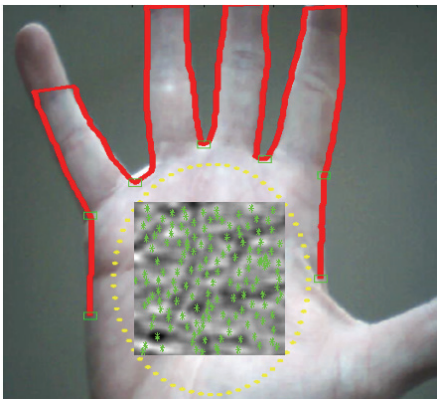

Fig. 13. Invariant area of the hand palm and the MSIFT features overlapped to the palm

Step 4. **Orientation assignment:** In our experiments we had used 16 orientations for each keypoint location based on local image gradient directions. For an image sample $L(x,y)$ at scale σ, the gradient magnitude, $m(x,y)$, and orientation, $\theta(x,y)$, are processed using pixel differences

$$m(x,y) = \sqrt{(L(x+1,y) - L(x-1,y))^2 + (L(x,y+1) - L(x,y-1))^2} \tag{21}$$

$$\theta(x,y) = \tan^{-1}\left(\frac{L(x,y+1) - L(x,y-1)}{L(x+1,y) - L(x-1,y)}\right) \tag{22}$$

Keypoint descriptor: Around each keypoint, the local gradients are measured at the selected scale to obtain a descriptors vector $\{d_i\}_{i=1}^{M}$ with M keypoints. Once the keypoints are extracted, the query image is matched and compared with each of the features extracted with the corresponding images in the registration database (from the training feature sets). The verifier evaluates the number of matches between a questioned and the training images. Let $\{d_i^t\}_{i=1}^{M}$ and $\{d_i^q\}_{j=1}^{L}$ be the set of training and questioned keypoint descriptors respectively. The distance between keypoint descriptors is calculated from:

$$D_d(i,j) = \left\| d_i^t - d_j^q \right\|^2 \tag{23}$$

Where $\|\cdot\|$ is the Euclidean norm. We define a match between a training d_i^t and a questioned d_i^q keypoint when:

$$1.5 D_d(i,j) < \min\{D_d(i,n)\}_{n=1}^{L} \tag{24}$$

with $n \neq j$. The threshold is estimated heuristically during the training stage and it is not particularly sensitive to values in the range of 1.2 to 1.7.

Matches Validation: matches validation is common on fingerprint and other biometric feature approaches. In this chapter we propose a validation based on coordinates distance between keypoints to improve the SIFT performance on contactless palmprint biometrics. The hypothesis is that the coordinates from two keypoints matched must be similar if we correct the average displacement from all the matches. Let $c_i^t = \{x_i^t, y_i^t\}_{i=1}^{M}$ and $c_j^q = \{x_i^q, y_i^q\}_{i=1}^{L}$ be the set of training and questioned keypoint coordinates respectively. The distance between coordinates is calculated from:

$$D_c(i,j) = \left\| c_i^t - c_j^q \right\|^2 \tag{25}$$

where $\|\cdot\|$ is the Euclidean norm. We define a match between a training c_i^t and a questioned c_i^q keypoint when

$$D_c(i,j) \leq \frac{1.5}{M} \sum_{i=1}^{M} \left\| c_i^t - c_j^q \right\|^2 \tag{26}$$

Due to high pose variance in contactless imaging we used a 1.5 weight factor to allow small alignment errors between palms.

The maximum number of matches between the questioned and the training set is the similarity score. If the similarity score is grater than a threshold, the questioned image is autheticated.

5. Scores combination

Combining scores obtained from different procedures is a usual way of improving the performance of a biometric scheme. In this section we propose a method to combine the scores obtained from Geometry, MSIFT and OLOF. Figure 14 shows the distribution of genuine and imposter matching scores from the three feature extraction approaches. We can ascertain that the matching scores from the both features are widely separated. The distribution of matching scores also suggests that the matching scores from the two matchers are likely to be uncorrelated and therefore more effectively employed for combination.

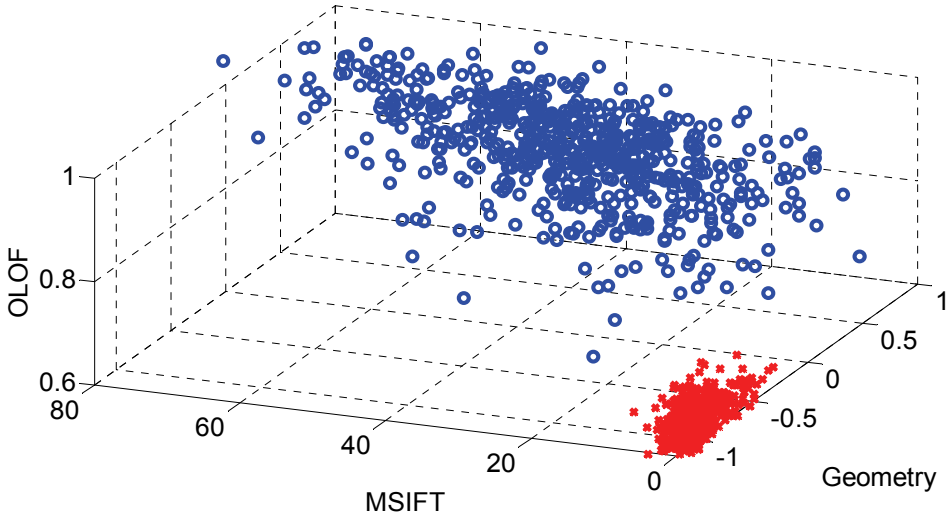

Fig. 14. Scores distributions for genuines (blue) and impostors (red) obtained for geometry, OLOF and MIFT.

Previous to combinate scores, we normalize the LSVM scores and OLOF scores based on *max/min* approach (Jain et al, 2005). The scores coming from the Hamming distance are not normalized. Now, it is possible to combine them at score level fusion based on a linear score combination functions as:

$$s_{comb} = ws_{geom} + (1-w)s_{palm} \tag{27}$$

Where s_{geom}, and $s_{palm} = (s_{OLOF} + s_{MSIFT})/2$ are the scores obtained with the image acquired in the visible and IR band respectively, w is the weighting factor and s_{comb} is the combined score which will be used for verify the input identity.

The value of w is obtained as follows. Let $s^g_{geom}(i)$ and $s^g_{palm}(i)$, $1 \le i \le N_g$ the scores of the genuine training samples in the visible and IR band respectively. A genuine score is obtained using two features vectors from the same user. Let $s^f_{geom}(i)$ and $s^f_{palm}(i)$, $1 \le i \le N_f$ the scores of the impostor training samples of in the visible and IR band respectively. An impostore score is obtained using features vectors from two different users (user x try to spoof the identity of user y). A distance measure between the distribution of genuine and impostor scores is obtained in visible band as follows:

$$\Delta_{geom} = (m^g_{geom} - m^f_{geom})^T \sum (m^g_{geom} - m^f_{geom}) \tag{28}$$

where the means are calculated as:

$$m^g_{geom} = \sum_{i=1}^{N_g} s^g_{geom} \Big/ N_g \tag{29}$$

$$m^f_{geom} = \sum_{i=1}^{N_f} s^f_{geom} \Big/ N_f \tag{30}$$

And $\Sigma = (\Sigma^g_{geom} + \Sigma^f_{geom})/2$ with $\Sigma^g_{geom} = \Sigma_{i=1}^{N_g} (s^g_{geom}(i) - m^g_{geom})^2 / N_g$ and $\Sigma^f_{geom} = \Sigma_{i=1}^{N_f} (s^f_{geom}(i) - m^f_{geom})^2 / N_f$ the covariance matrixes.

The distance between genuine and forgeries for the palm scores Δ_{palm} is obtained in the same way. The weighting factor is obtained as: $w = \Delta_{palm} / (\Delta_{palm} + \Delta_{geom})$.

6. Experiments and analysis

The database acquired with the proposed device consists of 1000 images captured in one session of 100 users. The image was acquired automatically in a supervised experiment.
Each experiment was performed as follows. We randomly selected four hands from each user to train and left the remaining hands for testing. Table 1 list the average EER rates after repeating the procedure ten times.

Features	EER
Geometry	0.88%
Palmprint OLOF	0.98%
Palmprint MSIFT	0.31%
Score Fusion	0%

Table 1. Averaged EER Obtained by the Hand Biometric System

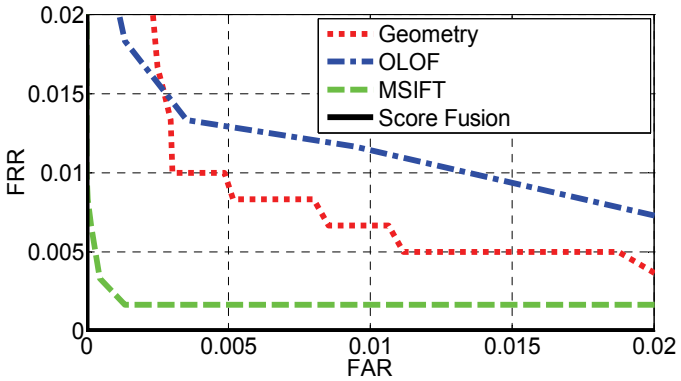

Fig. 15. DET curves of the proposed device. Dotted line: DET curve of geometrical device. Dash Dotted line: DET curve of OLOF features. Discontinuous line: DET curve of MSIFT features. Continuous line: DET curve of the combined scheme (OLOF+SIFT-Geometry).

The results show how MSIFT outperform OLOF and Geometry approaches. Geometry approach show better performance than OLOF. The fusion of all biometrics improves the performance with 0% of EER with our database.The DETs curves can be seen at Fig 15.

6.1 Computational time comparison

An analysis of the computational load of the biometric device is considered. Table 2 provides the executions times using a Dual Core processor at 1.66GHz programmed in the Matlab language for obtaining the geometric and palm texture parameters, the verification time, and (for the case of the analyzed scheme) the time that the ASM model toke to segment the hand in the visible image. Working with just the geometry, the analyzed devices answer in less than 1 second, which is appropriate for real time applications. In the case of IR plus visible images it takes less than 3 seconds, which should be speed up for real time applications.

Features	Run Time
Geometry	0.52 sec.
ASM	2.11 sec.
OLOF	0.07 sec.
MSIFT	1.51 sec.
Verification	0.38 sec.

Table 2. Time Consuming for Parameter Extraction and verification

7. Conclusions

This chapter has proposed a bispectral hand biometric system which acquires hand images in visible and IR band. The acquisition devices are two webcams, one per band, and the hand aquisition is contactless.The database used was built in an operational environment with a supervised enrollment.

The infrared images were used for geometric measures and the visible image for palmprint parameterization. An Active Shape Model was used to segment the hand in the visible image and a Least Square Support Vector Machine performed verification. An equal error rate of 0% was obtained combining biometries at score level.

Table 3 presents a summary of the most promising related work on contactless hand authentication.

Reference	Methodology	Database	Subjects	EER(%)
(Kumar 2008)	**Cohort Information**	**IITD (public)**	**235**	**1.31%**
(Hao et al, 2008)	**Multispectral Palmprint**	**Proprietary**	**165**	**0.5%**
This Chapter	**Geometry, Texture**	**Proprietary**	**100**	**0.0%**

Table 3. Releated work on contactlesshand authentication

8. Acknowledgment

This work has been supported by Spanish government project TEC2009-14123-C04.

9. References

Badrinath G. S. & Gupta P. (2009) "Robust Biometric System Using Palmprint for Personal Verification" *in Proceedings of International Conference on Biometrics*, Vol. 558, (2009), pp. 554-565.

Bulatov Y; Ambawalikar S. J. Kumar P. & Sethia S. (2004) "Hand Recognition using Geometric Classifiers", in *International Conference on Bioinformatics and its Applications*, Florida (December 2004).

Cootes T.F.; Taylor C.J.; Cooper D.H. & Graham J. (1995) "Active Shape Models – Their Training and Application", in *Computer Vision and Image Understanding*, Vol. 61, No. 1, (January 1995), pp. 38-59.

Doi J. and Yamanaka M. (2003) "Personal authentication using feature points on finger and palmer creases," *in the 32nd Applied Imagery Pattern Recognition Workshop*, (2003), Washington D.C.

Ferrer M. A.; Morales A.; Travieso C. M.; Alonso J. B. (2007) "Low cost multimodal biometric identification system based on hand geometry, palm and finger print texture" *in Proceedings of the 41st Annual IEEE International Carnahan Conference on Security Technolology*, (2007), pp. 52-58.

Haeger S. (2003) "Feature Based Palm Recognition", *Technical Report Univ. South Florida.* Tampa, (December 2003) Florida.

Han C. C.; Cheng H.L.; Lin C.L.; & Fan K.C. (2003) "Personal Authentication using palm print features", in *Pattern Recognition*, vol. 36, (2003), pp. 371-381.

Hao Y.; Sun Z.; Tan T. & Ren C. (2008) "Multi-spectral palm image fusion for accurate contact-free palmprint recognition," *in Proceedings of International Conference on Image Processing*, (2008), pp. 281-284.

Jain A. K.; Ross A. & Büke B. (1999) "A Prototype Hand Geometry based Verification System", in *Proceedings o 2nd International Conference on Audio and Video Based Biometric Person Authentication,* March 1999, pp. 166-171.

Jain A.K.; Bolle R. & Pankanti S. (2001) *Biometrics: Personal Identification in Networked Society*, Kluwer Academic Publishers, 2001.

Jain A. K.; Nandakumar K. & Ross A. (2005) "Score normalization in multimodal biometric systems" *Pattern Recognition*, (2005), vol. 38.

Kong W.K. & Zhang D. (2004) "Competitive Coding Scheme for Palmprint Verification," *in Proceedings of the 17th International Conference on Pattern Recognition*, vol.1, (2004), pp. 520-523.

Konga A.; Zhang D. & Kamelc M. (2009) "A survey of palmprint recognition", in *Pattern Recognition*, vol. 42, 2009, pp. 1408-1418.

Kumar A.; Wong D.C.M; Shen H.C. & Jain A.K. (2003) "Personal Verification using Palmprint and Hand Geometry Biometrics", *in Proceedings of the 4th International Conference on Audio and Video Based Biometric Person Authentication*, (June 2003).

Kumar A. & Zhang D. (2004) "Integrating shape and texture for hand verification", in *Proceedings of Third International Conference on Image and Graphics*, (2004), pp.222-225.

Kumar A.; Wong D.C.M.; Shen H.C. & Jain A.K. (2006) "Personal authentication using hand images", in *Pattern Recognition Letters*, vol. 27, no.13, (2006), pp. 1478-1486.

Kumar A. (2008) "Incorporating Cohort Information for Reliable Palmprint Authentication," *in Proceedings of Indian Conference on Computer Vision, Graphics and Image Processing*, Bhubaneswar (India), (December 2008), pp 112-119.

Li Q.; Qiu Z. & Sun D. (2006) "Feature-level fusion of hand biometrics for personal verification based on Kernel PCA", in *Proceedings of International Conference on Biometrics*, (2006), pp 744-750.

Lowe D. G. (2004) "Distinctive image features from scale-invariant keypoints" on International Journal of Computer Vision, vol. 2, no. 60, (2004), pp. 91 110.

Morales A.; Ferrer M. A.; Alonso J.B.; Travieso C. M. (2008) "Comparing infrared and visible illumination for contactless hand based biometric scheme," *in Proceedings of the 42nd Annual IEEE International Carnahan Conference, on Security Technology*, (2008). pp. 191 – 197.

Morales A.; Ferrer M. A. & Kumar A. (2010) "Improved Palmprint Authentication Using Contactless Imaging"*in Proceedings of the Fourth IEEE International Conference on Biometrics Theory, Applications and Systems*, (September 2010), Washington.

Öden C.; Erçil A.; & Büke B. (2003) "Combining implicit polynomials and geometric features for hand recognition", *in Pattern Recognition letters*, vol. 24, (2003), pp. 2145-2152.

Ribaric S.; Ribaric D. & Pavesic N. (2003) "Multimodal biometric user-identification system for network-based applications", in *IEEE Proceedings, Vision, Image and Signal Processing*, vol. 150, no.6, (2003), pp. 409-416.

Ribarić S. & Fratric I. (2005) "A Biometric Identification System Based on EigenPalm and EigenFinger Features", in *IEEE Transactions on Pattern Analysis and Machine Intelligence"*, vol. 27, no. 11, (November 2005), pp. 1698-1709.

Sanchez-Reillo R.; Sanchez-Avila C. & Gonzalez-Marcos A. (2000) "Biometric identification through hand geometry measurements," *IEEE Trans. Pattern Analysis and Machine Intelligence*, vol. 22, no. 10, (2000), pp. 1168–1171.

Sun Z., Tan T.; Wang Y. & Li S. Z. (2005) "Ordinal palmprint representation for personal identification,"*in Proceedings of IEEE Computer Society Conference on Computer Vision and Pattern Recognition*, vol. 1, (2005), pp. 279- 284.

Suykens J. A. K.; Gestel T. V.; Brabanter J. D.; Moor B. D. & Vandewalle J. (2002) "Least Squares Support Vector Machines" *World Scientific PublishingCo.*, Pte, Ltd (2002).

Travieso Carlos M; Alonso J. B., David S. & Ferrer Miguel A. (2004) "Optimization of a biometric system identification by hand geometry" *in Proceedings of Complex systems intelligence and modern technological applications*, Cherbourg, France, (September 2004), pp. 581-586.

Wong A. & Shi P. (2002) "Peg-free hand geometry recognition using hierarchical geometry and shape matching," in *Proceedings of IAPR Workshop on Machine Vision Applications*, Nara, Japan, (December 2002), pp. 281–284.

Yörük E.; Konukoglu E.; Sankur B. & Darbon J. (2006) "Shape-Based Hand Recognition", in *IEEE Transactions on Image Processing*, vol. 15, no. 7, (July 2006), pp. 1803-1805.

Zheng G.; Wang C.-J.; and Boult, T. E. (2007) "Application of Projective Invariants in Hand Geometry Biometrics", *IEEE Transactions on nformation Forensics and Security,* vol. 2, no. 4, (December 2007), pp. 758-768.